Extended depth of field microscopy for rapid volumetric two-photon imaging

Gabrielle Thériault,[1,2] **Yves De Koninck,**[1,2] **and Nathalie McCarthy**[1,*]

[1]*Département de physique, de génie physique et d'optique, Centre d'optique, photonique et laser (COPL), Université Laval, Québec (QC), Canada, G1V 0A6*
[2]*Centre de recherche Université Laval Robert-Giffard, Québec (QC), Canada, G1J 2G3*
[*]*nathalie.mccarthy@phy.ulaval.ca*

Abstract: Two-photon fluorescence microscopy is an influential tool in biology, providing valuable information on the activity of cells deep inside the tissue. However, it is limited by its low speed for imaging volume samples. Here we present the design of a two-photon scanning microscope with an extended and adjustable depth of field, which improves the temporal resolution for sampling thick samples. Moreover, this method implies no loss of optical power and resolution, and can be easily integrated into most commercial laser-scanning microscopy systems. We demonstrate experimentally the gain in performance of the system by comparing volumetric scans of neuronal structures with a standard versus an extended depth of field system.

OCIS codes: (180.4315) Nonlinear microscopy; (180.5810) Scanning microscopy.

References and links

1. F. Helmchen and W. Denk, "Deep tissue two-photon microscopy," Nat. Methods **2**, 932–40 (2005).
2. E. Beaurepaire, M. Oheim, and J. Mertz, "Ultra-deep two-photon fluorescence excitation in turbid media," Opt. Comm. **188**, 25–29 (2001).
3. W. Denk, J. H. Strickler, and W. W. Webb, "Two-photon laser scanning fluorescence microscopy," Science **248**, 73–76 (1990).
4. W. R. Zipfel, R. M. Williams, and W. W. Webb, "Nonlinear magic: multiphoton microscopy in the biosciences," Nat. Biotechnol. **21**, 1369–1377 (2003).
5. G. D. Reddy, K. Kelleher, R. Fink, and P. Saggau, "Three-dimensional random access multiphoton microscopy for functional imaging of neuronal activity," Nat. Neurosci. **11**, 713–720 (2008).
6. W. Göbel, B. M. Kampa, and F. Helmchen, "Imaging cellular network dynamics in three dimensions using fast 3D laser scanning," Nat. Methods **4** 73–79 (2007).
7. B. F. Grewe, D. Langer, H. Kasper, B. M. Kampa, and F. Helmchen, "High-speed in vivo calcium imaging reveals neuronal network activity with near-millisecond precision," Nat. Methods **7**, 399–405 (2010).
8. E. J. Botcherby, C. W. Smith, M. M. Kohl, D. Débarre, M. J. Booth, R. Juškaitis, O. Paulsen, and T. Wilson, "Aberration-free three-dimensional multiphoton imaging of neuronal activity at kHz rates," PNAS **109**, 2919–2924 (2012).
9. J. H. McLeod, "The axicon: a new type of optical element," J. Opt. Soc. Am. **44**, 592–597 (1953).
10. N. Olivier, A. Mermillod-Blondin, C. B. Arnold, and E. Beaurepaire, "Two-photon microscopy with simultaneous standard and extended depth of field using a tunable acoustic gradient-index lens," Opt. Lett. **34**, 1684–1686 (2009).
11. E. J. Botcherby, R. Juškaitis, and T. Wilson, "Scanning two photon fluorescence microscopy with extended depth of field." Opt. Commun. **268**, 253–260 (2006).
12. P. Dufour, M. Piché, Y. De Koninck, and N. McCarthy, "Two-photon excitation fluorescence microscopy with a high depth of field using an axicon," Appl. Opt. **45**, 9246–9252 (2006).
13. F. O. Fahrbach, P. Simon, and A. Rohrbach, "Microscopy with self-reconstructing beams," Nature Photon. **4**, 780–785 (2010).

#183366 - $15.00 USD Received 11 Jan 2013; revised 8 Mar 2013; accepted 14 Mar 2013; published 16 Apr 2013

14. T. A. Planchon, L. Gao, D. E. Milkie, M. W. Davidson, J. A. Galbraith, C. G. Galbraith, and E. Betzig, "Rapid three-dimensional isotropic imaging of living cells using Bessel beam plane illumination," Nature Meth. **8**, 417–423 (2011).
15. A. T. Friberg, "Stationary-phase analysis of generalized axicons," J. Opt. Soc. Am. A, **13**, 743–750 (1996).
16. T. A. Pologruto, B. L. Sabatini, and K. Svoboda, "ScanImage: flexible software for operating laser scanning microscopes," Biomed. Eng. Online **2**, 13 (2003).
17. O. Brzobohatý, T. Čižmár, and P. Zemánek, "High quality quasi-Bessel beam generated by round-tip axicon," Opt. Express **16**, 12688–12700 (2008).
18. H. Lütcke and F. Helmchen, "Two-photon imaging and analysis of neural network dynamics," Rep. Prog. Phys. **74**, 086602 (2011).

1. Introduction

In recent years, two-photon fluorescence microscopy has become an indispensable tool in the field of neuroscience, where it enables the functional imaging of cells deep inside the intact brain [1, 2]. For this type of microscopy, an ultrashort pulsed laser beam is focused so tightly that the fluorescent molecules present in the focal spot simultaneously absorb two photons and, in turn, act as a light source [3]. The excitation volume is therefore limited to the focal point, which leads to a high resolution in the image plane, but it is only present in a thin slice of the sample, an effect called optical sectioning [4]. Although optical sectioning is generally considered useful since it guarantees a uniform resolution throughout the sample, it reduces the acquisition speed for volume samples since one must acquire a stack of images at different depths to image the entire volume. In other words, the high spatial confinement has become a limitation for fast imaging of multiple, interacting cells such as in small neuronal networks.

As this limitation is growing ever more important in the field of neuroscience, the need for faster techniques increases and many approaches have been proposed. For example, high speeds approaching the kHz regime can be obtained by rapidly skipping from one point of interest to another in the volume with acousto-optic deflectors [5, 6], user-defined line-scans [7] or remote-controlled z-scanning [8], although these techniques require a prior mapping of the complete volume beforehand.

Another interesting approach to increase the imaging speed for volume samples is to spread the focal spot in the axial direction, creating a needle of light inside the sample. With this extended depth of field, less scans are required to probe the entire volume of interest. Various approaches have been presented in the past to extend the depth of field for two-photon microscopy by either rapidly displacing the focus with a photoacoustic lens [10] or using nondiffractive beams [11, 12]. A disadvantage of the photoacoustic lens is that it induces aberrations and the transverse resolution is not constant. On the other hand, nondiffractive beams have the advantage of offering the same transverse resolution at all depths. Such beams have also been generated for two-photon light-sheet microscopy by using a spatial light modulator [13] or an annular aperture [14]. Unfortunately, all the above methods imply losses of power because of unwanted diffractive orders [13], blocking with an annular aperture [11, 14], or power outside the sample [12]. In addition to these power losses, working with an extended focal spot spreads the remaining laser power over a large distance along the optical axis, and the signal strength accordingly decreases. It is therefore important in high depth of field systems to optimize the power throughput of the microscope and to adjust the depth of field to the sample's thickness. A last but equally important point to consider is the scanning method. In fact, achieving fast imaging relies on the ability to scan the laser beam. Previous attempts at generating extended depth of field microscopes with nondiffractive beams did not scan the beam (only the sample) [11, 12], which significantly limited the temporal resolution of such systems. The design we present here now overcomes this limitation, improving the temporal resolution from thick samples.

#183366 - $15.00 USD Received 11 Jan 2013; revised 8 Mar 2013; accepted 14 Mar 2013; published 16 Apr 2013

To image volume samples faster without deteriorating the transverse resolution of the final image, we designed a system that offers the ability to control the depth of field of excitation without compromising on resolution. Through the use of nondiffractive beams, our system extends the focal spot in the axial direction, which enables us to obtain the image of an entire volume with a single scan and ensures the transverse resolution to be constant throughout the volume. Our system also minimizes the power losses since we use a refractive axicon (conical lens) [9], which does not require spatial filtering, and anti-reflexion coatings on the axicon can further optimize transmission. Furthermore, we integrated the axicon in a standard two-photon scanning microscope in such a way that the depth of field of the microscope can be customized, and therefore adapted to the sample of interest. Hence, our system offers faster scanning speeds for volume samples, while optimizing the fluorescence signal. This strategy has the potential of dramatically enhancing temporal resolution to enable decoding of activity from multiple interacting neurons dispersed in a 3D network.

In this paper, we show that by adding a refractive axicon to a standard two-photon microscope, we can increase and adjust its depth of field, and therefore obtain the image of an entire volume with a single scan. First, we will present theory on the nondiffractive beams generated by axicons, and then show how such an element can be integrated in a standard laser-scaning microscope set-up. Next, we will present the flexibility of this system and prove that the experimental set-up produces the extended depth of field and constant resolution that the theory predicts. Finally, we will show two volume samples that we imaged using this extended depth-of-field microscope and demonstrate the increase in speed achieved by comparing volumetric scans of the standard system versus the extended depth of field system.

2. Using axicons to shape light

In standard laser-scanning microscopy, a Gaussian beam is focused inside the sample. Gaussian beams are diffractive, which means that above and below the focal plane, the beam rapidly widens. To extend the depth of field of the microscope while maintaining a good transverse resolution, we use a nondiffractive beam which can be generated from Gaussian beams with a simple optical element called axicon. In this section, we will present the equations that describe the laser beam after an axicon and we will highlight the parameters that control resolution and depth of field. We will then show how these relations are modified when the axicon is integrated in a scanning microscopy system to produce a needle of light inside the sample. Finally, we will show how the fluorescence signal strength varies when the depth of field is adjusted.

Axicons are refractive lenses shaped as a cone [9], often defined by the angle α between the sloped and plane faces. If a plane wave were incident upon an axicon, it would be deviated towards the optical axis by an angle β, defined as $\beta = \sin^{-1}(n\sin\alpha) - \alpha$, where n is the refractive index of the axicon (Fig. 1). Since all the rays are deviated towards the optical axis z with the same azimuthal angle, two phenomena occur. In the transverse plane, the interference pattern modulates the intensity as a zero-order Bessel function, which is characterized by an intense central lobe. Moreover, this pattern is nondiffractive, *i.e.* the central lobe has a constant radius.

In practice, a more accurate description of the nondiffractive beam produced by an axicon is the Bessel-Gauss beam. In fact, the intensity distribution of Gaussian beam transformed by an axicon can be obtained from the Fresnel diffraction integral by using the stationary phase approximation [15]:

$$I(r,z) = I_0 \frac{4\pi^2\beta^2 z}{\lambda} \exp\left(\frac{-2\beta^2 z^2}{w_0^2}\right) J_0^2\left(\frac{2\pi r\beta}{\lambda}\right), \tag{1}$$

where I_0 is the intensity at the center of the incident beam, β is the deviation angle of the axicon, λ is the wavelength, w_0 is the initial Gaussian beam width, z is the optical axis and r is

#183366 - $15.00 USD Received 11 Jan 2013; revised 8 Mar 2013; accepted 14 Mar 2013; published 16 Apr 2013

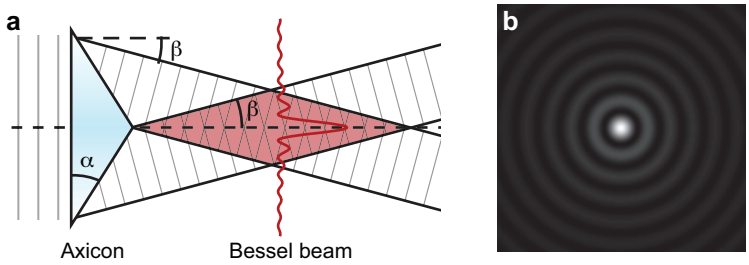

Fig. 1. **An axicon produces a nondiffractive beam. (a)** Schematic representation of an axicon (conical lens) of angle α illuminated by a plane wave. After the axicon, the interference pattern generates a Bessel beam, characterized by the deviation angle, β. The radial profile of a Bessel beam is traced in red. **(b)** Transverse intensity profile of a Bessel beam.

the radial coordinate. From this equation, we can see that the transverse distribution is shaped as a Bessel function and is invariant along the z-axis. Therefore, the beam is nondiffractive and its transverse resolution is controlled by the deviation angle β.

We define the transverse resolution of the Bessel-Gauss beam as the size of the central lobe or, more precisely, the radius ρ at the first zero of the Bessel function:

$$\rho = \frac{2.4048\lambda}{2\pi\beta}. \tag{2}$$

This value also corresponds to the full width at half-maximum of the signal point-spread function for two-photon fluorescence in the transverse plane.

Another useful parameter that can be extracted from Eq. (1) is the on-axis distance along which the central lobe is intense enough to produce a contrasted fluorescence signal: the effective depth of field, L. We define L as the full width at half-maximum of the signal point-spread function along the optical axis. The effective depth of field is directly proportional to $I(r=0,z)$ in single-photon fluorescence and to the squared intensity in two-photon fluorescence:

$$L = C\left(\frac{w_0}{\beta}\right), \tag{3}$$

where the constant C has a value of 0.8 for single-photon fluorescence and 0.58 for two-photon set-ups. From this relation, one can observe that if a system allows for a variation in the initial Gaussian beam width w_0 incident on the axicon, it will result in a variation of the depth of field (which is proportional to w_0) while keeping constant the transverse resolution of the Bessel-Gauss beam. It is therefore possible to independently control the depth of field and the transverse resolution of the beam by varying only the angle of the axicon and the width of the incident beam.

For example, in a typical case of a small network of neurons in a sample rat brain slice, the desired parameters for the excitation volume could be a transverse resolution of 1 μm with a depth of field of 100 μm. From Eqs. (2) and (3), we can calculate that this would require an axicon with an angle $\alpha = 30°$, illuminated by a Gaussian beam of width $w_0 = 65$ μm. Such a small beam only illuminates the very tip of the axicon, and with the current manufacturing processes, it is extremely difficult to produce a high-angle axicon with a perfect tip. Fortunately, when we insert an axicon into a laser-scanning microscope set-up, it can be judiciously positioned so that magnification factors enable us to use a wider beam and a lower-angle axicon, which lowers the demands on the precision of the axicon.

#183366 - $15.00 USD Received 11 Jan 2013; revised 8 Mar 2013; accepted 14 Mar 2013; published 16 Apr 2013

In our system, we placed a Fourier-Transform lens after the axicon to produce an annulus of light with radius $R = f_\alpha \tan\beta$, where f_α is the focal length of the lens (Fig. 2). This annulus is relayed through the scanning system and imaged onto the back focal plane of the microscope objective. The objective then transforms the annulus of light back into a Bessel-Gauss beam and scales it down. The intensity distribution at the sample therefore has the same shape as expressed in Eq. (1), but because of the magnification we must replace w_0 and β by w_f and β_f:

$$w_f = \frac{w_0 F}{m f_\alpha} \tag{4a}$$

$$\beta_f = \tan^{-1}\left(\frac{m f_\alpha \tan\beta}{F}\right), \tag{4b}$$

where F is the effective focal length of the microscope objective and m is the magnification applied to the annulus of light while being relayed to the objective. The same substitutions apply in Eqs. (2) and (3). Since these relations were obtained using small angle approximations, they are only valid for objectives with low numerical apertures. For objectives with high numerical apertures, the vector nature of the electromagnetic field should be considered when calculating the intensity distribution [11].

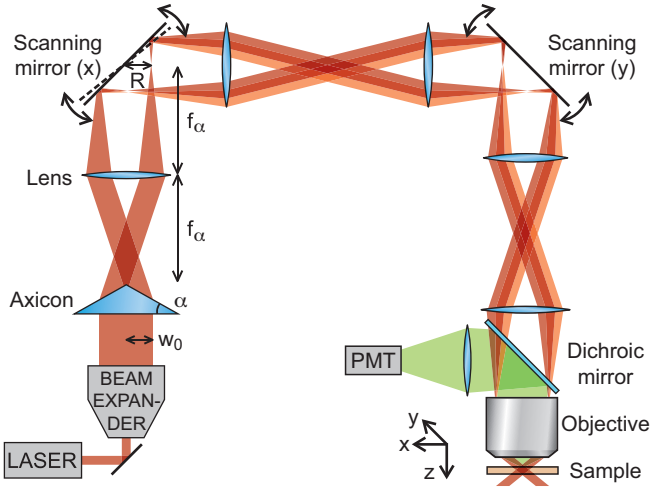

Fig. 2. **Schematic of the set-up.** A Ti:Sapphire laser illuminates an axicon of angle α followed by a lens (focal length f_α), which transform the laser beam into an annulus of light of radius R. This annulus is imaged into the back focal plane of the objective lens, which creates a tightly focused Bessel-Gauss beam in the sample. The scanning system (in our case a pair of galvanometric mirrors and relay lenses) enables a beam tilt in the back focal plane of the objective, leading to an x-y scan of the beam in the sample. Fluorescence light is retro-collected with the objective and directed to a photomultiplier tube (PMT) with a dichroic mirror.

In the Introduction, we mentioned that when a focal spot is extended to increase the depth of field, the fluorescence intensity decreases. Let us now verify how this relationship can be expressed mathematically. Considering that the total power of the input Gaussian beam is $P = I_0 \pi w_0^2/2$, the substitution of P and L in Eq. (1) yields the following equation for the on-axis intensity distribution:

$$I(r=0,z) = \frac{8\pi P z}{\lambda}\left(\frac{C}{L}\right)^2 \exp\left(\frac{-2z^2C^2}{L^2}\right). \tag{5}$$

#183366 - $15.00 USD Received 11 Jan 2013; revised 8 Mar 2013; accepted 14 Mar 2013; published 16 Apr 2013

A partial derivative of Eq. (5) with respect to z shows that the maximum intensity is proportional to P/L. It follows that for two-photon fluorescence, in which all the fluorescence signal comes from the focal line, if the depth of field is doubled (with constant laser power and transverse resolution), the fluorescence signal strength decreases by a factor 4.

3. Results

Using the theory presented above, we built a scanning two-photon microscope (Fig. 2) which allows the insertion of an axicon and its Fourier-transform lens at the entrance of the scanning system. The scanning system is composed of a set of closed-loop galvanometric mirrors (Cambridge Technologies, 6215HM40B) linked by a pair of achromatic doublets of equal focal length and relayed to the microscope objective with a scale factor $m = f_3/f_2 = 1.5$. The laser is a Ti:Sapphire laser (Mira, Coherent) with a maximum available power of 900 mW, tuned to a central wavelength of 850 nm in the mode-locked regime. A dichroic beamsplitter (Semrock, 705 nm edge BrightLine) allows the laser light to reach the sample through the objective lens (Zeiss, Plan-Neofluar 20X, 0.5NA and Zeiss, W N-Achroplan 40X, 0.75 NA) and reflects the fluorescence towards a photomultiplier tube (Hamamatsu, R3896). The galvanometric mirrors and data collection was performed with the ScanImage software [16]. A telescope arrangement was also used to adjust the beam width illuminating the axicon (w_0), and we used uncoated UVFS axicons with angles $\alpha = 2.5$ degrees and $\alpha = 5$ degrees, fabricated by Altechna.

In this section, we will present the flexibility of our system and prove that the experimental set-up produces the extended depth of field and constant resolution that the theory predicts. Finally, we will show two samples that we imaged and demonstrate the increase in speed achieved by comparing volumetric scans of standard versus extended depth of field systems.

3.1. Measuring the point-spread function

The extended depth of field microscope we have presented here offers a good transverse resolution and enables us to vary the depth of field. We validate the technique both theoretically and experimentally by calculating and measuring the point-spread function (PSF) of the microscope for two different depths of field.

The PSF is an optical system's response to an infinitely small light source. In the case of a fluorescence microscope, the PSF describes the distribution of the excitation volume. To calculate our instrument's PSF in the longitudinal (x-z) plane, we considered that the collected signal is proportional to the square of the intensity presented in Eq. (1). For the results shown in Fig. 3, we used the following parameters: an axicon of angle $\alpha = 5^\circ$, a Fourier-Transform lens $f_\alpha = 60$ mm, an objective with a focal length $F = 8.25$ mm and a magnification ratio of $m = 1.5$, and we calculated the two-photon fluorescence distribution in the x-z plane for two different depths of field: $L = 36\ \mu$m with a Gaussian beam width $w_0 = 0.27$ mm (Fig. 3(d)) and $L = 63\ \mu$m with $w_0 = 0.47$ mm (Fig. 3(f)).

We obtained experimental measurements of the PSF by mounting fluorescent microspheres (Molecular Probes, Fluosphere 505/515, diameter 500 nm) on microscope slides with fluorescent mounting medium (Dako). Since the microspheres are smaller than the resolution of the laser beam, the collected signal is proportional to the square of the intensity presented in Eq. (1). We used the same parameters as in the calculations, and we acquired a stack of images by translating the sample 1 μm in the z direction between each acquisition (Figs. 3(e) and 3(g)).

The experimental PSFs show a very good agreement with the calculated ones. We observe in Fig. 3 that the experimental results present an axial distribution that is slightly less smooth than the theory predicts. Such variations of the on-axis intensity are probably caused by a slight curvature at the axicon apex [17]. Nevertheless, the central lobe maintains a constant resolution throughout the depth of field and the depth of field is very close to its theoretical value. Also,

#183366 - $15.00 USD Received 11 Jan 2013; revised 8 Mar 2013; accepted 14 Mar 2013; published 16 Apr 2013

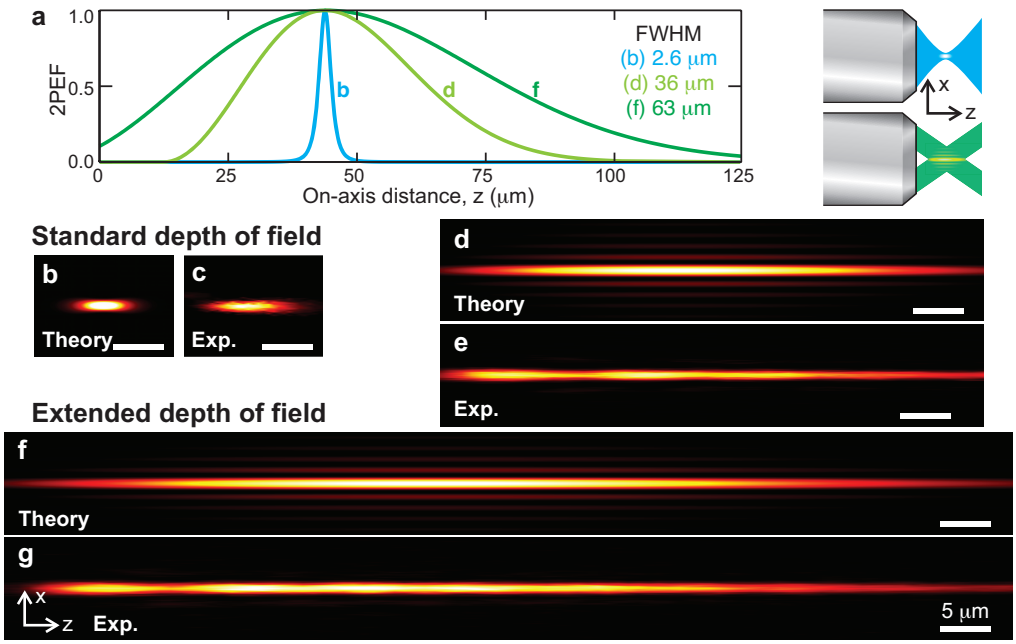

Fig. 3. **Longitudinal point-spread function. (a)** Two-photon excitation fluorescence (2PEF) signal along the z axis for an extended depth of field set-up (green) compared to a standard set-up (blue) with the same transverse resolution. **(b), (c)** Calculated and experimental PSF in the x-z plane with standard depth of field set-up ($w_0 = 2.7$ mm). **(d) to (g)** Calculated and experimental PSF in the x-z plane with extended depth of field set-ups ($w_0 = 0.27$ mm for d-e and $w_0 = 0.47$ mm for f-g). Experimental PSFs were measured with 500 nm fluorescent beads. See text for parameters used. Scale bars, 5 μm.

the sidelobes are less visible in the experimental results, which suggests that there will be very little background fluorescence noise.

Finally, the results presented in Fig. 3 validate the direct relationship between the depth of field and the width of the Gaussian beam (see Eq. (3)). When the only parameter that is changed in the set-up is the width of the Gaussian beam incident on the axicon, the transverse resolution of the microscope stays constant and only the depth of field is affected. On the other hand, if either the axicon, the Fourier-Transform lens or the objective lens were changed, then both the depth of field and the resolution of the microscope would be modified.

3.2. Extended depth of field imaging

We now show examples of images recorded using the extended depth of field microscope. For comparison purposes, we modified our system to enable us to acquire standard two-photon fluorescence images. This simple modification consists in removing the axicon and its Fourier-transform lens from the path of the laser beam, which is equivalent to using a standard two-photon microscope.

Our first test specimen is a block of 1% agarose in which fluorescent beads are suspended (Molecular Probes, diameter 3 μm). With the standard system, only a few spheres are imaged in each plane, and we had to acquire a stack of 13 scans to image all the spheres in the volume of interest, spanning a depth of 60 μm (Figs. 4(a) to 4(d)). The acquisition time for each frame was 1 s, with 512x512 pixels and a pixel dwell time of 4 μs, which are typical values for

#183366 - $15.00 USD Received 11 Jan 2013; revised 8 Mar 2013; accepted 14 Mar 2013; published 16 Apr 2013

laser-scanning two-photon microscopy [18].

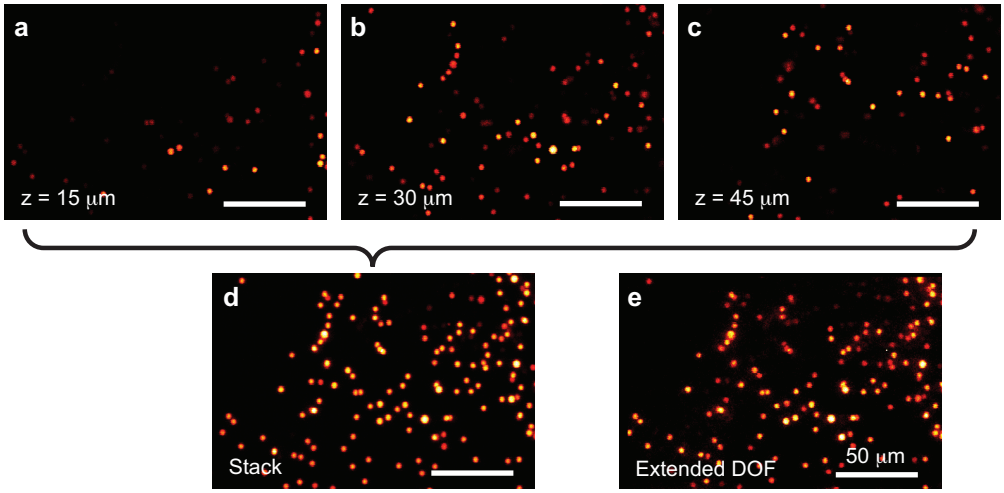

Fig. 4. **3-micron fluorescent polymer beads in agarose. (a)-(c)** Standard two-photon fluorescence images acquired at various depths by translating the sample. **(d)** Z-summed stack of 13 standard two-photon scans (including those shown in **a** to **c**), spanning a depth of 60 μm. **(e)** An extended depth of field image acquired in a single scan. See text for parameters used. Scale bars, 50 μm.

We then added the axicon and lens to achieve a depth of field of approximately 60 μm, using the same set of parameters as for Fig. 3(e) ($w_0 = 0.47$ mm, $\alpha = 5^\circ$, $f_\alpha = 60$ mm, $F = 8.25$ mm and $m = 1.5$). With a single frame scan and the same pixel dwell time, all the fluorescent spheres present in the volume were imaged (Fig. 4(e)). This demonstrates that the entire volume of interest was scanned in only one frame, which results in this case in a 13-fold increase in speed when compared to the standard method.

The extended depth of field two-photon microscope can also be used to image biological samples. As an example, we fixed a 100-micron thick rat brain slice and injected a hippocampal neuron with Lucifer Yellow. With the standard two-photon set-up, only parts of the dendrites can be observed in a single image (Fig. 5(a) to 5(c)). To image the complete dendritic tree we had to acquire 26 scans, spanning a depth of 50 μm (Fig. 5(d)). Once again, the acquisition time for each frame was 1 s, with 512x512 pixels and a pixel dwell time of 4 μs.

With the extended depth of field set-up, the same neuron was imaged using $w_0 = 0.7$ mm, $\alpha = 2.5^\circ$, $f_\alpha = 60$ mm and $F = 4.125$ mm (Fig. 5(e)). Although only one scan was needed to image the entire volume of interest, we averaged each line 5 times to improve the signal-to-noise ratio. In this case, the extended depth of field approach therefore leads to a 5-fold increase in speed. The limiting factor in this case was the available laser power. With higher peak intensities it would not have been necessary to average each line and the increase in scanning speed would have been 26-fold.

Both the stack average and the extended depth of field image show the same structures, whereas individual standard depth of field scans only show parts of the dendrites since they are located at different depths within the sample. This is illustrated by the intensity line scans inset in Fig. 5. The intensity profiles have the same shape for the averaged stack and the extended depth of field images, but the profiles from scans with the standard depth of field only show specific parts of the neuron.

#183366 - $15.00 USD Received 11 Jan 2013; revised 8 Mar 2013; accepted 14 Mar 2013; published 16 Apr 2013

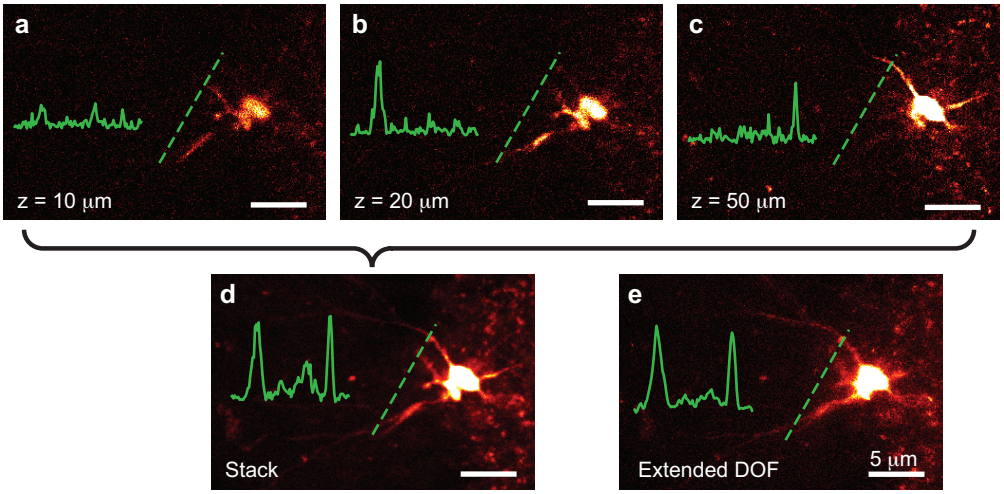

Fig. 5. **Rat hippocampal neuron in fixed brain slice, stained with Lucifer Yellow. (a)-(c)** Standard two-photon fluorescence images acquired at various depths by translating the sample. **(d)** Z-summed stack of 26 standard two-photon scans (including those shown in **a** to **c**), spanning a depth of 60 μm. **(e)** An extended depth of field image acquired in a single scan. **Inset curves:** Intensity line scans along the dashed lines. See text for parameters used. Scale bars, 5 μm.

4. Discussion

In conclusion, extended depth of field microscopy opens an entirely new perspective on volumetric imaging. We have shown that adding an axicon into a two-photon scanning microscope increases its depth of field by shaping the laser beam as a Bessel beam instead of a spot. This system offers the ability to control the depth of field of excitation without compromising on transverse resolution, while significantly improving the acquisition speed for a volume. Also, the extended depth of field brings forth new possibilities for in-vivo imaging, since small vertical movements (such as those caused by breathing) no longer bring the plane of interest out of focus. We believe that this approach will prove a critical advancement towards enabling neuroscientists to decipher the functional organization of complex neuronal networks; that is, the intact brain.

We also believe that the novel approach presented here will likely be adopted rapidly by the microscopy community because of its technical simplicity and its adaptability to existing microscopes. In fact, one must simply insert an axicon and a lens in the optical path of the laser so that an annulus of light is formed at the entrance of the beam-steering system (*i.e.* in the plane conjugate to the objective back focal plane). For example, we used a set of closed-loop galvanometric mirrors, but the scanning speed could be enhanced by replacing the fast-axis mirror by a resonant mirror or a spinning polygon disk, as long as the mirror plane is conjugate to the annulus of light. The system is thus fully retrofittable into existing commercial systems. This feature will likely result in a broad acceptance of the technology by the community, further amplifying and accelerating its impact.

Pertaining to future work, we are currently studying the possibility of replacing the Fourier-transform lens by an adjustable-focus lens. The depth of field and the transverse resolution of the microscope could therefore be adjusted depending on the thickness of the sample without having to replace and realign any of the optical elements. This would enhance the flexibility of

#183366 - $15.00 USD Received 11 Jan 2013; revised 8 Mar 2013; accepted 14 Mar 2013; published 16 Apr 2013

the extended depth of field microscope and optimize power yield at the sample.

Acknowledgments

This work was supported by the National Sciences and Engineering Research Council of Canada (NSERC), the Canadian Institutes of Health Research (CIHR), the Canadian Institute for Photonic Innovations (CIPI) and the Fonds de recherche du Québec – Nature et technologies (FQRNT).

#183366 - $15.00 USD Received 11 Jan 2013; revised 8 Mar 2013; accepted 14 Mar 2013; published 16 Apr 2013